Available online at www.sciencedirect.com
ScienceDirect
Acta Materialia 59 (2011) 4303–4313
Acta MATERIALIA
www.elsevier.com/locate/actamat

Effect of uniaxial loading on the structural anisotropy and the dynamics of atoms of $Cu_{50}Zr_{50}$ metallic glasses within the elastic regime studied by molecular dynamics simulation

Y. Zhang [a,*], N. Mattern [a], J. Eckert [a,b]

[a] IFW Dresden, Institute for Complex Materials, Helmholtzstr. 20, D-01069 Dresden, Germany
[b] TU Dresden, Institute of Materials Science, D-01062 Dresden, Germany

Received 9 November 2010; received in revised form 19 March 2011; accepted 20 March 2011
Available online 12 April 2011

Abstract

The changes in the structure and dynamics of atoms and the stress-induced structural anisotropy of a $Cu_{50}Zr_{50}$ metallic glass upon the application of uniaxial compressive and tensile stresses within the elastic regime during the loading and unloading processes have been studied using molecular dynamics simulation. The structural change is found to be more significant under tension than under compression, which is accompanied with the destruction of the full icosahedra clusters into distorted ones. Permanent structural change is found at the applied tensile stress of 1000 MPa but is still within the elastic regime. The fabric tensor and bond number analysis reveals that the structural anisotropy increases monotonously with the applied stress, being more pronounced along the loading direction than in the other two free directions. The results of the mean square displacement, the non-Gaussian parameter and the mobile atom analysis suggest that the dynamics of the atoms are distinctly different under uniaxial stresses above 800 MPa. The α-relaxation occurs more easily under tension than under compression as the applied stresses exceed 800 MPa. The permanent change in the structure and structural anisotropy could be correlated with the change in the dynamics of the atoms.

Keywords: Metallic glasses; Structural anisotropy; Elastic behavior; Molecular dynamics simulations

1. Introduction

Metallic glasses (MGs) have long been thought to be isotropic materials due to the absence of well-defined crystallography directions in comparison to crystalline materials [1,2]. However, sophisticated synchrotron diffraction experiments have revealed the existence of structural anisotropy (SA). SA exists in MGs after rapid solidification and becomes pronounced as these materials are mechanically deformed. The SA in $Zr_{57}Ti_5Cu_{20}Al_{10}Ni_8$ bulk metallic glasses (BMGs) induced by high-pressure torsion under room temperature was reported by Révész et al. [3], who found that a shift in position of the first maximum of the structure factor can be clearly observed on both the surface and the cross-section of the plastically deformed samples. It is well known that the plastic deformation of MGs is highly inhomogeneous at low temperatures and high strain rates, with the plastic flow mostly localized within very tiny shear bands of about 5–10 nm in size [4]. It is therefore very straightforward to associate the SA introduced by plastic deformation with the formation of shear bands. Interestingly, the presence of shear bands is not a requisite of SA. SA has also been found in various deformed homogeneous MGs without the occurrence of shear bands. Dmowski and Egami [5] studied the mechanical creep of an $Fe_{81}B_{13}Si_4C_2$ MG at 250 and 300 °C. Creep experiments were also performed by Ott et al. using a $Cu_{64.5}Zr_{35.5}$ BMG (under uniaxial compression) at 425 °C [6] and a $Zr_{41.2}Ti_{13.8}Cu_{12.5}Ni_{10}Be_{22.5}$ BMG (under uniaxial tension)

* Corresponding author. Tel.: +49 351 4659 686; fax: +49 351 4659 452.
E-mail address: yue.zhang@ifw-dresden.de (Y. Zhang).

1359-6454/$36.00 © 2011 Acta Materialia Inc. Published by Elsevier Ltd. All rights reserved.
doi:10.1016/j.actamat.2011.03.054

at 325 °C [7], respectively. The SA was clearly demonstrated by the difference in intensities between two measured geometries in all the above-mentioned cases. Moreover, it has been shown that SA can be identified even within the elastic regime, e.g. in $Cu_{50}Zr_{50}$ and $Cu_{64.5}Zr_{35.5}$ MGs upon uniaxial tension [8] and in a $Zr_{57}Ti_5Cu_{20}Ni_8Al_{10}$ BMG [9] upon uniaxial compression, respectively. The presence of SA within the elastic regime implies that the SA may be related to the early stage of formation of shear bands or the activation of shear transformation zones. An accurate characterization of SA is therefore very helpful both to underpin the understanding of the mechanism of SA and to control the deformation behavior of MGs.

The mechanism of SA was proposed by Egami et al. [10] to be the bond reorientation that takes place during deformation. According to Egami et al., the structure of glasses becomes anisotropic to memorize the effect of the deformation. Molecular dynamics (MD) simulations performed using a single-component glass with a modified Johnson potential and a binary glass with a Lennard-Jones potential showed that the SA is dominated by a sixfold term, indicating that bond reorientation can proceed by cutting a bond parallel to the applied stress and forming one in the perpendicular direction [11,12].

The structural evolution of deformed MGs below the yielding has also been extensively studied using MD simulation. Park et al. [13] simulated the structural change in $Cu_{50}Zr_{50}$, $Cu_{57}Zr_{43}$ and $Cu_{65}Zr_{35}$ MGs under compression using the Lennard-Jones 4–8 potential. They found that the fraction of full icosahedra (ICO) dropped significantly with increasing strain. A similar decrease in the fraction of full ICO was also observed in the $Cu_{65}Zr_{35}$ MG under simple shear by MD simulation using the same potential [14]. Furthermore, it was found that the disordering process of the structure is irreversible even if the applied shear stress is removed. The accommodation of uniaxial tensile strain in a $Cu_{46}Zr_{54}$ MG was studied by Lekka et al. [15] using a tight binding model. They reported that the numbers of ICO destroyed and created within the elastic regime are almost the same, resulting in a dynamically constant number of ICO clusters. Despite the numerous studies on the structure of deformed MGs, the dynamics of the atoms of MGs under deformation are less focused. Recently, a scaling relationship between the temperature and stress affecting the viscosity in a simulated $Zr_{50}Cu_{40}Al_{10}$ MG under shear was proposed by Guan et al. [16]. This indicates that the applied shear stress can also play an important role in the dynamic properties of MGs, which may be also applicable to the uniaxial loading mode.

In this study, we choose a simple binary alloy, $Cu_{50}Zr_{50}$, as a model system and perform MD simulation to shed light on the SA and the effect of applied uniaxial tensile and compressive stresses on the dynamics of atoms, including the loading and unloading process. The SA is characterized by the second-order contact fabric tensor, the anisotropic coefficient proposed by Rountree et al. [23] and the number of bonds with respect to the direction of loading. The structural analysis was performed by means of common-neighbor analysis with specified cut-offs for each atom pairs. The dynamics of the atoms was studied using the mean square displacement (MSD), the non-Gaussian parameter (NGP) and the analysis of mobile atoms. We find that a larger degree of SA can be introduced by tensile stresses than by compressive ones in the Simulated $Cu_{50}Zr_{50}$ MGs. Also, the dynamics of the atoms can be altered differently by compressive and tensile stresses. The change in the dynamics of the atoms in the simulated $Cu_{50}Zr_{50}$ MGs upon the application of uniaxial stresses is also presented.

2. Modeling and simulation

2.1. Molecular dynamics simulation

MD simulations were performed using the LAMMPS package [17]. The simulation box contains 3000 atoms. Since we did not intend to study the mechanism of plastic deformation in this study, we believed that such a box size is adequate to achieve both good statistic resolution and optimum computation time. The potential developed using the embedded atom method (EAM) of Kim and Lee [18] was employed. Periodic boundary conditions and constant pressure and temperature were used throughout the simulation process. The simulation step size was 2.5 fs.

The initial configuration of $Cu_{50}Zr_{50}$ was constructed using a random distribution of Cu and Zr atoms in a cubic simulation box according to the stoichiometry. The simulation box was held at 2000 K for 10 ns, then continuously cooled down to 300 K at a cooling rate of 10^{10} K s^{-1}. The resultant structure was relaxed at 300 K for 1 ns before any load was applied. The purpose of the relaxation was to remove the SA induced by the high cooling rate of the simulation to the greatest possible extent. All the components of the pressure tensor were set to zero during the melting and quenching processes, as well as during the relaxation.

Instead of the stepwise application of an external strain, we deformed the simulation box by controlling the components of the pressure tensor and checking the response of the simulation box. All components except the one parallel to the z direction of the simulation box (σ_{33}) were set to zero. Various constant pressures (200, 400, 600, 800, 1000, 1200 and 1300 MPa) were applied to the simulation box for 300 ps (loading), then the pressure was removed and the response of the simulation box was recorded for 300 ps (unloading). The applied stresses as a function of the simulation time are shown in Fig. 1. It can be seen that the stresses are almost constant throughout the loading process. However, some fluctuations can be identified as the applied stresses exceed 800 MPa. Therefore, the data of the first 20 ps of the loading process were ignored in order to eliminate the shockwave effect [19]. In total, 500 configurations were collected to perform the common neighbor analysis and the fabric tensor analysis, which are described in detail in Section 2.3. The results are then

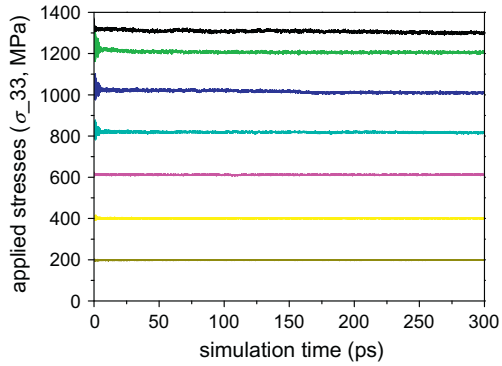

Fig. 1. The applied uniaxial stresses (tensile and compressive) along the z-direction of the simulation box as a function of the simulation time.

averaged and the error bars are obtained from the standard deviations.

2.2. Determination of strains

The strains are defined in terms of the change in the box lengths along the loading direction. The evolution of box lengths under compressive stresses of 200 and 1300 MPa with simulation time is illustrated in Fig. 2 as an example. It can be seen that the change in the lengths of the simulation box under the compressive stress of 200 MPa is almost fully recoverable and time independent. The instantaneous elastic strain, ε_{ie}, is defined using the immediate change in the simulation box with respect to its original value upon loading. The instantaneous elastic strain is observed to vanish immediately as the applied stress is removed. However, it can be seen that the change in the simulation box is time dependent under 1300 MPa. The anelastic strain, ε_{ae}, can be clearly observed from the time-dependent recovery of the simulation box upon unloading. The part of the remaining strain that decays beyond the simulation timescale is defined as being plastic (ε_p).

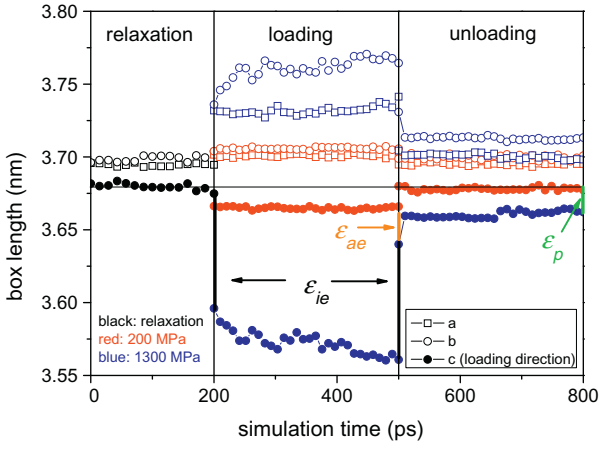

Fig. 2. The evolution of the box lengths during the relaxation, loading and unloading processes of the simulated $Cu_{50}Zr_{50}$ MG under compressive stresses of 200 (red) and 1300 MPa (blue), respectively, showing the definitions of the instantaneous elastic strain, the anelastic strain and the plastic strain. (For interpretation of the references to colour in this figure legend, the reader is referred to the web version of this article.)

2.3. Characterizations of structure and the structural anisotropy

Common neighbor analysis (CNA) has been extensively employed in analyzing the structure of glasses and crystals [20,21]. However, the cut-offs for each interatomic pair have to be carefully specified to obtain reliable results. In this study, the cut-offs of Cu–Cu, Cu–Zr and Zr–Zr interatomic pairs were set at 0.306, 0.323 and 0.366 nm, respectively, corresponding to the first minimum of the partial pair distribution functions (PDFs) shown in Fig. 3. It can be seen that the simulated total PDF reproduces the experimental result well [22].

The matrix of the fabric tensor (FT) $\boldsymbol{F}$ was constructed to characterize the SA. If the interatomic distance between two atoms is no larger than the cut-offs used in CAN, a pair of normal unit vectors $\boldsymbol{n}$ are constructed at the contact point. The relationship between $\boldsymbol{F}$ and $\boldsymbol{n}$ is $\boldsymbol{F} = \langle \boldsymbol{n} \otimes \boldsymbol{n} \rangle$, where the notation $\otimes$ means tensor product and the $\langle\rangle$ stands for the average over all vectors $\boldsymbol{n}$. The SA can be characterized by the three eigenvalues, $\boldsymbol{\lambda_i}$ ($i = 1, 2, 3$), of $\boldsymbol{F}$. Since the trace of $\boldsymbol{F}$ is unity or, equivalently, the sum of all three eigenvalues is unity, all the eigenvalues are equal to 1/3 for isotropic materials. However, a deviation of the eigenvalues from 1/3 can be observed when SA exists. The value of $\boldsymbol{\lambda_i}$ has been shown to be very sensitive to the SA [23]. The higher the degree of SA, the larger the deviation. The anisotropic coefficient, α, can be defined in terms of $\boldsymbol{\lambda_i}$ as:

$$\alpha = \frac{3}{\sqrt{6}} \left(\sum_{i=1}^{3} \left(\lambda_i - \frac{1}{3} \right)^2 \right)^{1/2} \quad (1)$$

It can be seen that α is zero for isotropic materials, whereas α is unity in the case of full anisotropy.

Besides the FT, we believe that the number of bonds parallel and perpendicular to the loading direction are direct measures of SA based on Egami's bond reorientation mechanism. The analysis of bond number was carried out

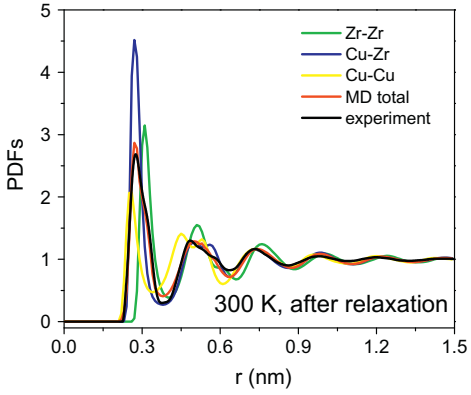

Fig. 3. The total and partial PDFs of the simulated $Cu_{50}Zr_{50}$ MG after relaxation at 300 K for 1 ns. The experimental total PDF is also presented.

as follows: first, all the possible bonds were identified under the periodic boundary condition. It was found that the total number of bonds (including Cu–Cu, Cu–Zr and Zr–Zr) fluctuates between 18,500 and 18,700 under all the applied stresses. Secondly, a counting sphere was constructed using the cut-offs in CNA (see Fig. 4). The total volume of the counting sphere was then divided into three sub-volumes: the volume within azimuth angles of ±15° with respect to the loading and free direction were assigned the counting volume of the loading and free direction, V_l and V_f, respectively. The rest was assigned as the "transition" direction (V_t). It can be deduced that $V_l{:}V_t{:}V_f = (1-\cos15°){:}(\cos15°-\sin15°){:}\sin15°$. Finally, all the bonds were categorized and counted with respect to each counting volume.

2.4. Analysis of dynamics of the atoms

The MSD, the NGP and the number of mobile atoms were employed to analyze the dynamics of the atoms in the simulated $Cu_{50}Zr_{50}$ MGs. The MSD is defined as:

$$\langle r^2(t)\rangle = \frac{1}{N}\sum_{1}^{N}\langle |r_i(t)-r_i(0)|^2\rangle \tag{2}$$

where N is the total number of atoms, $r_i(t)$ is the position of atom i at time t and $r_i(0)$ is its initial position. The NGP, $\alpha_2(t)$, is defined as:

$$\alpha_2(t) = \frac{3\langle r^4(t)\rangle}{5\langle r^2(t)\rangle^2} - 1 \tag{3}$$

where the $\langle r^2(t)\rangle$ is the MSD and $\langle r^4(t)\rangle$ is the mean quartic displacement. The qualitative behavior of NGP is well known from simulations. The NGP tends to zero as $t \to 0$ and rises on the picosecond scale typical for vibrations to a value of around 0.2. In hot liquids the NGP drops from this value whereas in undercooled liquids and glasses it keeps growing and reaches values an order of magnitude larger. Only on the timescale of diffusion or α-relaxation does the NGP drop and finally reach $\alpha_2(t) = 0$ as $t \to \infty$ [24].

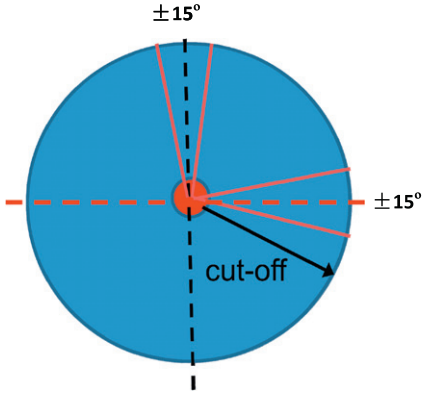

Fig. 4. Schematic drawing of the counting volumes used in the bond number analysis. The black and red dash lines refer to the loading and the free directions, respectively. (For interpretation of the references to colour in this figure legend, the reader is referred to the web version of this article.)

Mobile atom analysis has previously been used to identify the collective motions of atoms at the grain boundaries of nanocrystals [25–27]. Atoms are defined as being mobile if they move an interatomic distance in times where most of the atoms have not moved such a distance.

The criterion of the mobile atoms in this study is:

$$0.35r_0 < |r_i(\Delta t) - r_i(0)| < 0.85r_0 \tag{4}$$

where $r_i(0)$ is the initial position of atom i and $r_i(\Delta t)$ is its position after a time interval Δt. r_0 is the average interatomic spacing that corresponds to the first maximum of the partial PDFs. The lower bound in Eq. (4) is chosen to ensure that the movement of a mobile atom is larger than the average amplitude of thermal vibration and the upper bound is chosen to ensure that the movement is small compared to the diffusive distance.

3. Results and discussion

3.1. Stress–strain curves and volume change

The values of ε_{ie}, ε_{ae} and ε_p and the mean strain as a function of the applied stresses are shown in Fig. 5. It can be seen that all the strains under compression and tension are almost identical when the stresses applied are below 800 MPa. Above 800 MPa, all the strains under tension are larger than those under compression and the discrepancy becomes more pronounced with increasing stresses. The ε_{ie} exhibits the best linear relationship with respect to the applied stress and the smallest discrepancy between the tension and compression. The elastic modulus determined using ε_{ie} is around 56.5 GPa, which is about 70% of the experimental value of the $Cu_{50}Zr_{50}$ BMG [28]. It can be seen in the figure that ε_{ae} increases with the applied stresses, being linear as a function of the applied stresses under all compressive stresses and under tensile stresses below 800 MPa. ε_{ae} increases significantly under tension as the applied stresses exceed 800 MPa, ending up with a value about twice as large as that under compression at 1300 MPa. Fig. 5 also shows that ε_p is small under both compression and tension below 1000 MPa, indicating that the yielding of the simulated $Cu_{50}Zr_{50}$ MG occurs between 1000 and 1200 MPa, which is in accordance with the results of Lekka et al. [15]. The plastic strain rises significantly above 1000 MPa, being four times as large under tension as under compression at 1300 MPa. As a consequence, the mean strain deviates from a linear relationship with respect to the applied stresses above 1000 MPa. It should be pointed out that the experimental flow stress of $Cu_{50}Zr_{50}$ BMGs is approximately 1500 MPa, which is 200 MPa larger than the maximum pressure applied in this study. The discrepancy between the simulation and the experiments may be caused on the one hand by the inadequateness of the EAM potential and on the other hand by

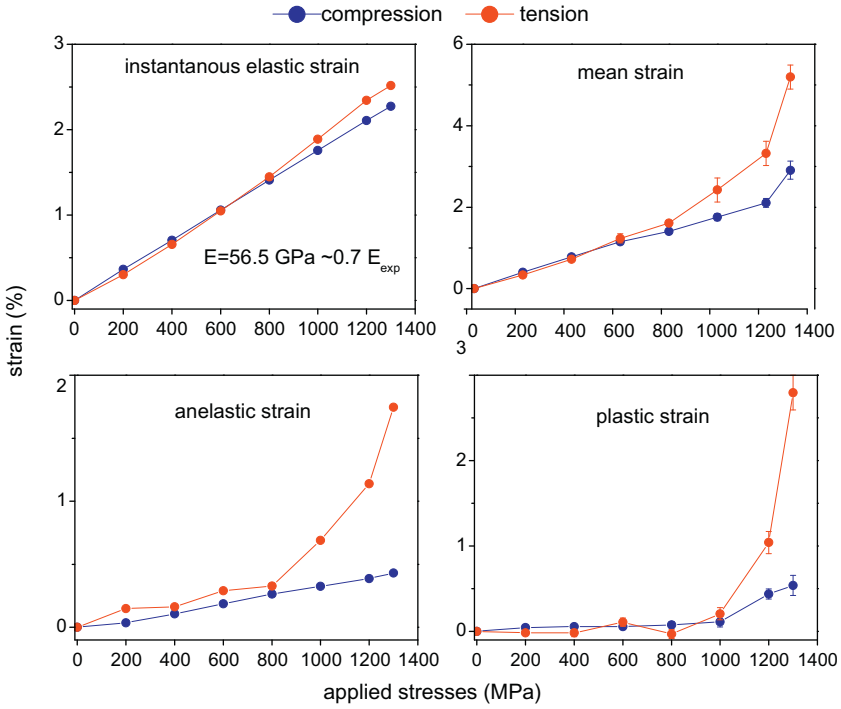

Fig. 5. The instantaneous elastic strain, anelastic strain, plastic strain and mean strain of the simulated $Cu_{50}Zr_{50}$ MG under various uniaxial tensile and compressive stresses.

the high quenching rate used in the MD simulation, which has already been demonstrated in a simulated $Zr_{47}Cu_{46}Al_7$ by the decrease in the shear strength with higher quenching rates [29]. The discussion below will focus on the results obtained under stresses below 1000 MPa (i.e. within the elastic regime); the results obtained under stresses above 1000 MPa are presented mostly for comparison purposes.

The evolution of the volume as a function of the simulation time is presented in Fig. 6a. It can be seen that the volume of the simulated $Cu_{50}Zr_{50}$ MG expands upon tension and contracts upon compression due to Poisson's effect. The volume change can be almost fully recovered after the compressive or tensile stresses are removed, even with the presence of the plastic strain. The volume change under all the compressive and tensile stresses is illustrated in Fig. 6b. It can be seen that the volume change as a function of the applied stresses is almost linear under both compression and tension. Below 200 MPa, the volume changes under compression and under tension are almost identical. However, the volume changes more rapidly under tension than under compression within the range of 200–1000 MPa, being −0.23% and 0.32% under compressive and tensile stresses of 1000 MPa, respectively. The volume change under uniaxial stresses is very small comparing to that at the melting points of most simple metals (around 3–7%), which is only of the order of the change in the free volume of BMGs annealed under the glass transition temperature by thermoanalysis [30] or density measurements [31].

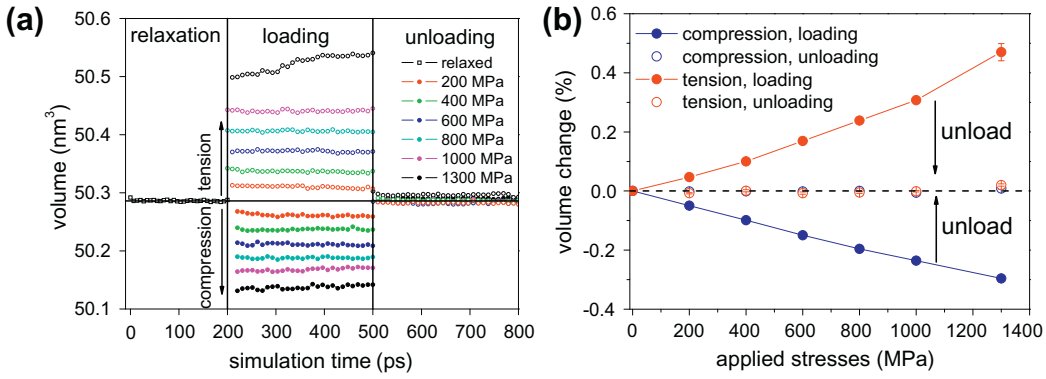

Fig. 6. (a) The evolution of the volume of the simulated $Cu_{50}Zr_{50}$ MG under various uniaxial tensile and compressive stresses as a function of the simulation time during the relaxation, loading and unloading processes. (b) The corresponding volume change as a function of the applied stresses.

3.2. Structural change

It has been shown that CNA is a powerful tool with which to analyze the local structures of both nanocrystals and glasses. The bond pair with an index of (1551) is related with the full ICO cluster, while the distorted ICO cluster can be indexed by (1541) or (1431). The (1421) and (1422), (1441) and (1661) bond pairs are characteristic of face-centered cubic (fcc)/hexagonal close-packed (hcp)-like and body-centered cubic (bcc)-like structures, respectively. The CNA results of the simulated $Cu_{50}Zr_{50}$ MG under various uniaxial tensile and compressive stresses are presented in Fig. 7. It can be seen that the fractions of both the full and the distorted ICO are almost constant under all compressive stresses below 1000 MPa during both the loading and unloading processes, whereas a decrease in (1551) can be clearly observed under tensile stresses between 600 and 1000 MPa. The increase in the fraction of the distorted ICO under tension can be understood as a consequence of the consumption of the full ICO. Nevertheless, the absolute value of the change in the fraction of full ICO is relatively small (~0.5%), corresponding to 6.7% with respect to the fraction of full ICO in the relaxed structure. The fractions of both the full and distorted ICO return to their initial values upon unloading, when the applied compressive and tensile stresses do not exceed 1000 and 800 MPa, respectively. This indicates that the movement of the atoms involved in the elastic deformation is relatively small in the simulated $Cu_{50}Zr_{50}$. However, a permanent change within the simulation timescale in the structure can be observed at the applied tensile stress of 1000 MPa, indicating that the local structures change greatly. It can be seen that the fraction of the fcc/hcp-like cluster increases upon compression and decreases upon tension. This is probably due to the contraction of the volume under compression, where the fcc/hcp-like structure, with its denser packing, is preferred. The change in the fraction of the fcc/hcp-like clusters is fully reversible upon unloading. The fraction of the bcc-like clusters is about 5–10 times smaller than that of the fcc/hcp-like clusters and can be considered as almost constant under all compressive and tensile stresses (fluctuations within 0.05%).

3.3. Structural anisotropy

The SA is characterized using the three eigenvalues of the fabric tensor and the anisotropic coefficient, as illustrated in Fig. 8. The deviations of λ_i ($i = 1, 2, 3$) from 1/3 directly reflect the SA along the x, y and z axes of the simulated $Cu_{50}Zr_{50}$ MG, respectively. It can be seen that λ_i is very close to 1/3 after relaxation, indicating that the structure is very close to the isotropic state after relaxation. However, all the eigenvalues deviate from 1/3 upon the application of compressive and tensile stresses, showing the stress-induced structural anisotropy. The most significant change is found along the loading direction, i.e. the z axis of the simulation box, corresponding to λ_3. It is found that the value of λ_3 changes more rapidly under tension than under compression, indicating that tensile stresses induce more pronounced SA than compressive stresses of the same magnitude. The values of λ_i return to their initial values when the applied compressive and tensile stresses are below 1000 and 800 MPa, respectively. However, the values of λ_i cannot restore their initial values within the simulation timescale at the applied tensile stress of 1000 MPa. The anisotropic coefficient of the configuration at 300 K after quenching at 10^{10} K s^{-1} is about 7.5×10^{-4} and shows almost no change upon further

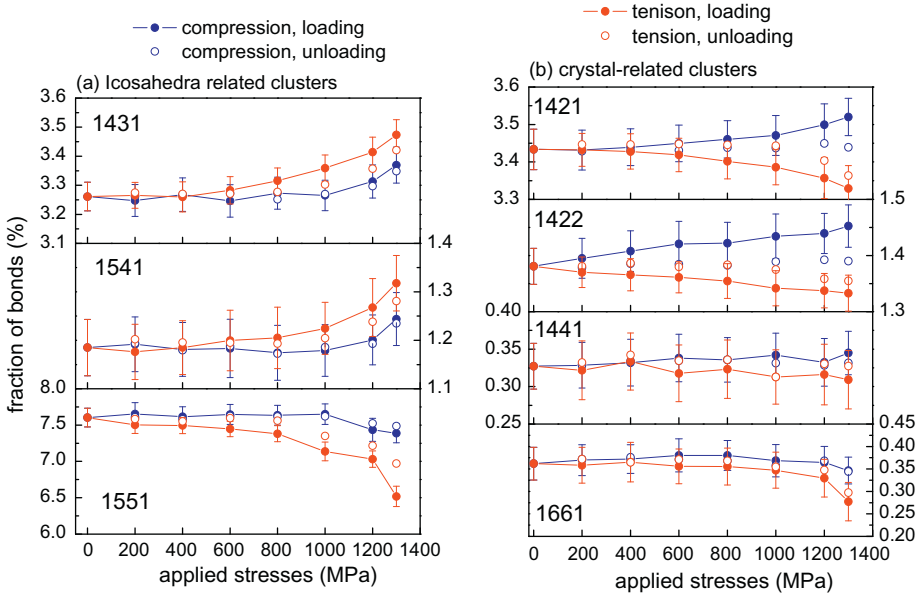

Fig. 7. The average fractions of (a) the ICO-related clusters and (b) the crystal-related clusters in the simulated $Cu_{50}Zr_{50}$ MG as a function of the applied uniaxial stresses, including the loading and unloading processes.

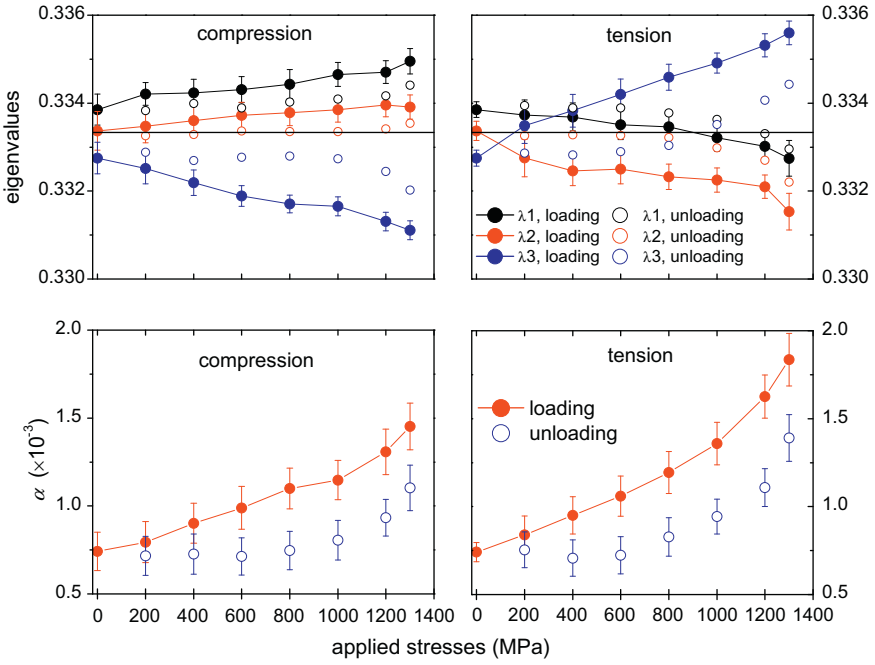

Fig. 8. The eigenvalues of the fabric tensor and the anisotropic coefficient of the simulated $Cu_{50}Zr_{50}$ MG under constant uniaxial stresses, including the loading and unloading processes.

relaxation at 300 K. As a comparison, the anisotropic coefficient of the liquid $Cu_{50}Zr_{50}$ at 2000 K was 1.8×10^{-4}. The anisotropic coefficient shows a monotonous increase as a function of the applied stresses, being comparable under tension and under compression below 600 MPa. It is clearly seen that the value of the anisotropic coefficient is larger under tension than under compression as the applied stresses exceed 800 MPa. The anisotropic coefficient restores its initial value after the compressive stress is removed, implying that the stress-induced SA by compressive stresses below 1000 MPa can be fully recovered. Nevertheless, the residual anisotropic coefficient after the removal of the tensile stress of 1000 MPa indicates a permanent SA.

The distributions of Cu–Cu, Cu–Zr and Zr–Zr bonds along the free, transition and loading directions under all the applied compressive and tensile stresses are shown in Fig. 9. Some general features can be observed: first, the changes in the fractions of all types of bonds along the loading and free directions show opposite behavior, e.g. the numbers of bonds increase along the free direction but decrease along the loading direction under compression; secondly, the fractions of all types of bonds along the same direction exhibit opposite behavior under compression and tension, e.g. the fractions of all the bonds rise under compression but descend under tension along the free direction; thirdly, the fractions of all types of bonds within the transition direction show fluctuating behavior under both compression and tension. This is in good agreement with the deformation mechanism of MGs within the elastic regime proposed by Egami et al., namely, bonds along the compression direction tend to break and form along the free direction to accommodate the external stress, whereas the tendency is the opposite under tension. The change in the fraction of the bonds within the transition direction is probably due to the large number of bonds within the counting volume, so that a relatively small change in the bond fractions is enshrouded. Upon unloading, the fractions of bonds go back to their initial values as the applied compressive and tensile stresses are below 1000 and 800 MPa, respectively. However, the number of bonds cannot return to the original value under a tensile stress of 1000 MPa. This is in accordance with the results of the CNA and the fabric tensor analysis, indicating that a permanent SA has been introduced in the $Cu_{50}Zr_{50}$ simulated MG under the tensile stress of 1000 MPa by the destruction of the full ICO clusters into distorted ICO clusters to an irreversible extent within the elastic regime.

3.4. Dynamic of the atoms

The MSD traces of Cu and Zr atoms under compression and tension as a function of the simulation time are shown in Figs. 10 and 11, respectively. The time dependence of the MSD shows the following features: (i) the MSD of Cu atoms is larger than that of Zr atoms under all conditions due to the atom size effect, i.e. the smaller Cu atoms are more mobile than the Zr atoms; (ii) for short times ($t < 10$ ps), the MSD increases by the quadratic dependence on relaxation time due to the ballistic motion of the atoms; (iii) for intermediate times, a plateau on all the MSD traces due to the so-called "cage effect" appears as the applied stresses are below 1000 MPa, i.e. each atom is surrounded by an effective cage formed by its neighbors that confines

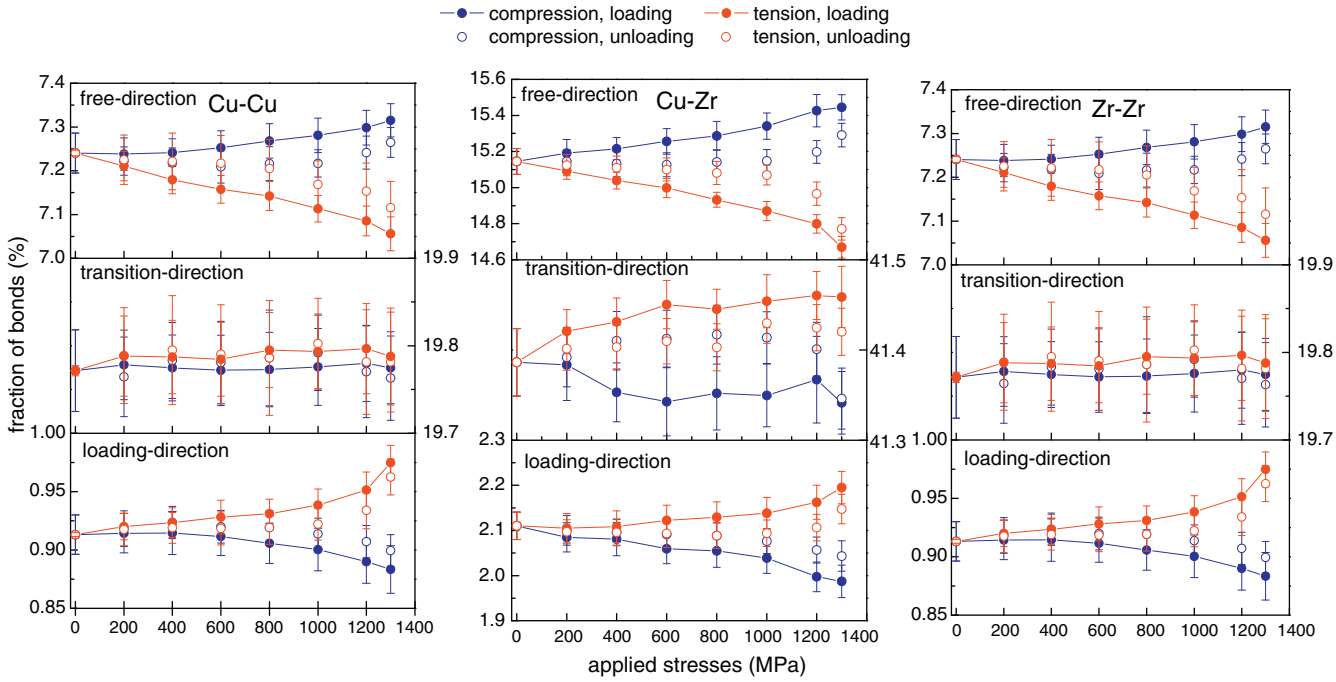

Fig. 9. The fractions of the Cu–Cu, Cu–Zr and Zr–Zr bonds along the loading, transition and free directions of the simulated $Cu_{50}Zr_{50}$ MG under various uniaxial tensile and compressive stresses during the loading and unloading processes.

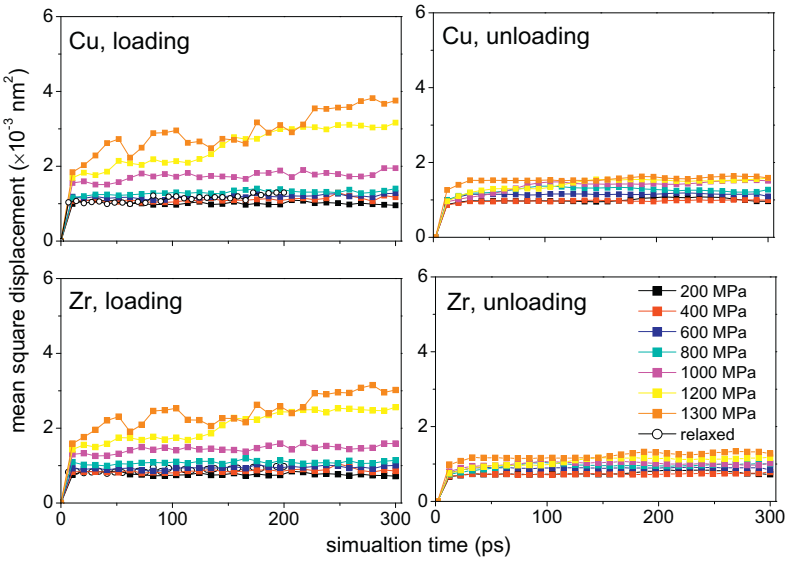

Fig. 10. The MSD of the Cu and Zr atoms as a function of the simulation time of the simulated $Cu_{50}Zr_{50}$ MG under various uniaxial compressive stresses during the loading and unloading processes.

the atom to movement close to its original position; and (iv) the atom succeeds in leaving the cage only after a sufficiently long time, resulting in a diffusive motion with a characteristic linear dependence of MSD on time, which can be observed as the applied stresses exceed 1000 MPa. It can be seen that the MSD traces of the simulated $Cu_{50}Zr_{50}$ MG under compression and tension below 800 MPa almost overlap with the relaxed sample at 0.001 nm^2, indicating that the dynamics of atoms are quite similar under these loading conditions. The level of the plateau of the MSD traces at a stress of 1000 MPa at intermediate times is comparable to those at stresses below 1000 MPa under both compression and tension. However, an increase in the MSD to 0.015 nm^2 can be observed at long times – at about 180 and 70 ps under compression and tension, respectively – indicating that the atoms escape their surrounding cages more easily under tension than under compression at a stress of 1000 MPa. Upon unloading, the plateaus of all the MSD traces drop back to a similar level of around 0.001 nm^2.

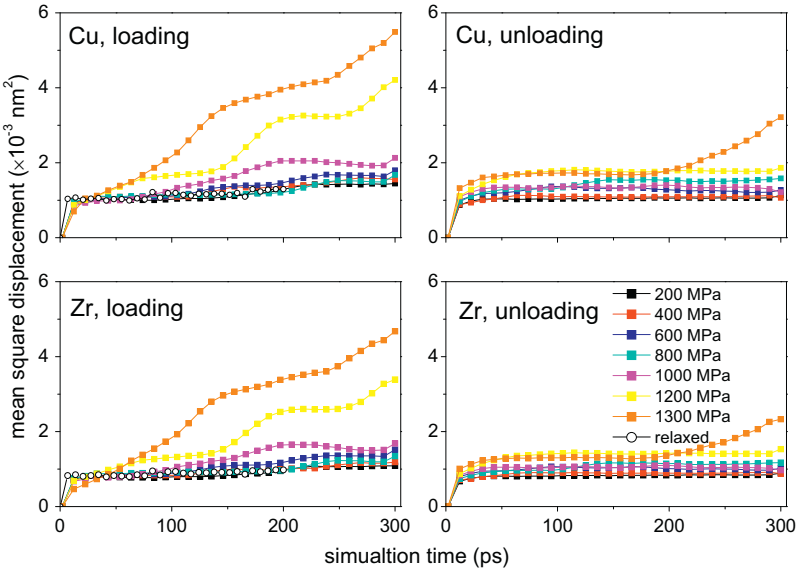

Fig. 11. The MSD of the Cu and Zr atoms as a function of the simulation time of the simulated $Cu_{50}Zr_{50}$ MG under various uniaxial tensile stresses during the loading and unloading processes.

The NGPs of the simulated $Cu_{50}Zr_{50}$ MG under compression and tension as a function of the simulation time are shown in Fig. 12 and 13, respectively. It is found that the NGP is very close to zero at short times (less than 10 ps). The NGP can be fitted well as a function of the square root of the simulation time, as proposed by Caprion et al. [24], at intermediate times within the range of 10–100 ps under all the compressive and tensile stresses, followed by a peak at long times. It can be seen that the amplitude of the NGP is quite similar under tension and under compression as the applied stresses are below 800 MPa, whereas the NGP is larger under tension than under compression at 1000 MPa, indicating a higher degree of dynamics heterogeneity. The peak in the NGP profile is shown to be closely correlated with the timescale of α-relaxation. It can be observed that the peak of the NGP shifts to longer simulation time under both compression and tension as the applied stresses are below 600 MPa, indicating the confinement of the atoms to perform diffusive movement. However, it can be seen that the peak shifts to shorter simulation time as the applied stresses exceed 800 MPa, being more significant under tension than under compression. This implies that the atomic structure has undergone distinct rearrangements during which the cages become less rigid, therefore the α-relaxation takes place more easily. The NGP exhibits a plateau after the peak

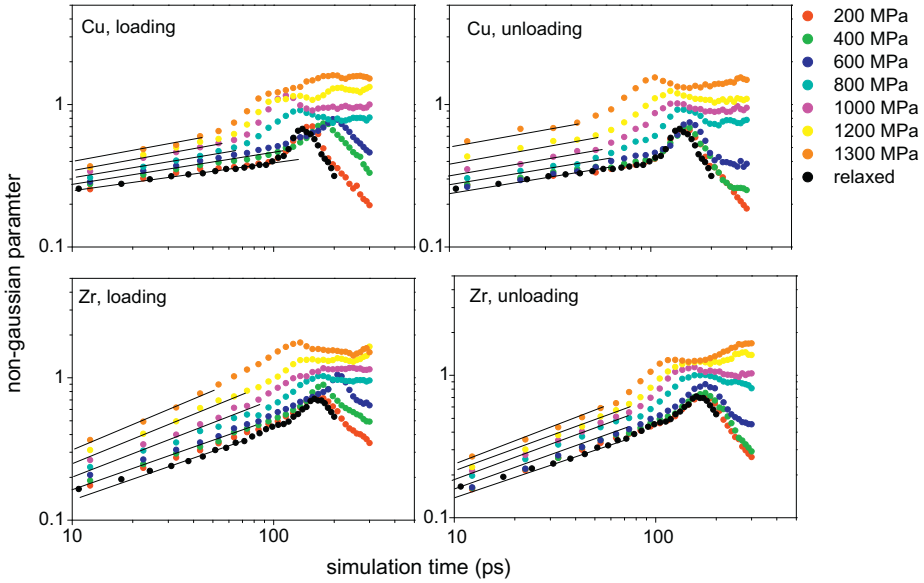

Fig. 12. The NGP of the Cu and Zr atoms of the simulated $Cu_{50}Zr_{50}$ MG under various uniaxial compressive stresses during the loading and unloading processes.

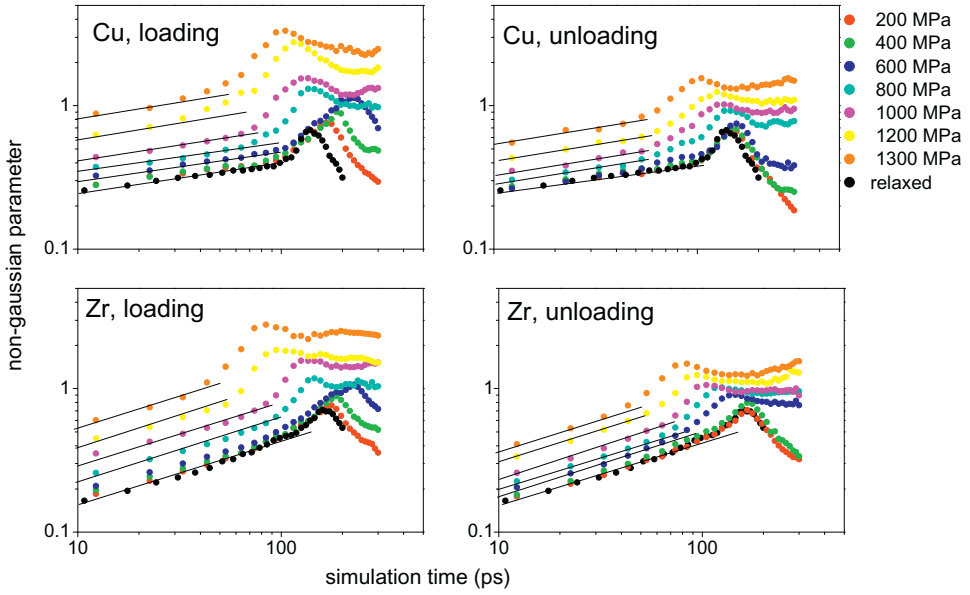

Fig. 13. The NGP of the Cu and Zr atoms of the simulated $Cu_{50}Zr_{50}$ MG under various uniaxial tensile stresses during the loading and unloading processes.

as the applied stresses exceed 600 MPa instead of gradual descending back to zero, showing a higher degree of dynamics heterogeneity that is beyond the timescale of the MD simulation. The NGP profiles are quite similar under both compression and tension upon unloading, when the position of the peak shifts back and overlaps with that of the relaxed sample as the applied stresses are below 600 MPa. However, a delay in the descent of the NPG can be observed at an applied stress of 600 MPa, indicating that the effect of uniaxial stress on the dynamics of atoms is irreversible. The position of the NGP peak cannot return to the value of the relaxed samples at applied stresses of 800 and 1000 MPa, implying a more significant change in the dynamics of the atoms.

The result of the mobile atom analysis is shown in Fig. 14. It can be seen that the numbers of mobile atoms are almost constant and very small under both compressive and tensile stresses below 800 MPa. However, an increase in the number of mobile atoms can be clearly identified as the applied stresses exceed 1000 MPa, being 6- and 40-fold larger under tension and compression, respectively, compared with the value of the relaxed sample. The mobile atoms may emerge at places where local shear or α-relaxation occurs due to the collective movement of several atoms. All the results of the MSD, NGP and mobile atoms analysis suggest that the dynamics of the atoms can be altered when uniaxial compressive or tensile stresses are applied in the simulated $Cu_{50}Zr_{50}$ system. The physical nature of this process may be related to (i) the volume change and (ii) the change in the potential energy landscape of the simulated $Cu_{50}Zr_{50}$ MG upon the application of uniaxial stresses. Actually, the disappearance of local potential energy minima in a simulated glass upon the application of shear stresses has been already shown by Malandro and Lacks [32]. In addition, it has been demonstrated that the dynamics of the atoms are closely related to the fraction of full ICO in Cu–Zr MGs [33]. The results in this study indicate that not only the fractions but also the stress state of the full ICO can impact the dynamics of atoms in Cu–Zr MGs, which is worthy of further investigation.

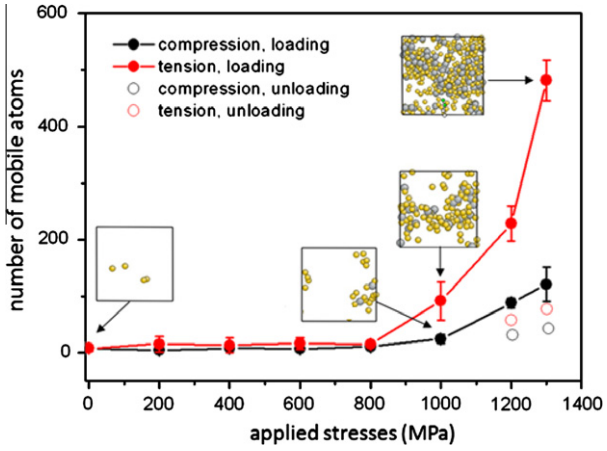

Fig. 14. The number of mobile atoms in the simulated $Cu_{50}Zr_{50}$ MG under various uniaxial tensile stresses during the loading and unloading processes. The numbers of mobile atoms during the unloading process below 1000 MPa are almost identical to the data indicated by the black line and symbol, which are not presented for clarity.

4. Summary and conclusions

In this study, the structural change and stress-induced structural anisotropy of a $Cu_{50}Zr_{50}$ metallic glass upon the application of uniaxial compressive and tensile stresses within the elastic regime during the loading and unloading

processes have been studied using molecular dynamic simulation. It is found that the structural change is more significant under tension than under compression, which is accompanied by the destruction of full icosahedra clusters into distorted ones. Permanent structural change is found at an applied tensile stress of 1000 MPa but is still within the elastic regime. Fabric tensor and bond number analysis reveals that the structural anisotropy increases monotonously with applied stress, which is more pronounced along the loading direction than in the other two free directions. The results of the mean square displacement, the non-Gaussian parameter and the mobile atom analysis suggest that the dynamics of the atoms are distinctly different under higher uniaxial stress above 800 MPa compared to lower ones. The α-relaxation occurs more easily under tension than under compression as the applied stresses exceed 800 MPa. The permanent change in the structure and structural anisotropy could be correlated with the change in the dynamics of the atoms upon the application of uniaxial stresses.

References

[1] Inoue A. Acta Mater 2000;48:279.
[2] Takayama S. J Mater Sci 1976;11:164.
[3] Révész A, Schafler E, Kovacs Z. Appl Phys Lett 2008;92:011910.
[4] Schuh CA, Hufnagel TC, Ramamurty U. Acta Mater 2007;55:4067.
[5] Dmowski W, Egami T. J Mater Res 2007;22:412.
[6] Ott RT, Heggen M, Feuerbacher M, Park ES, Kim DH, Kramer MJ, et al. Acta Mater 2008;56:5575.
[7] Ott RT, Kramer MJ, Besser MF, Sordelet DJ. Acta Mater 2006;54:2463.
[8] Mattern N, Bednarcik J, Pauly S, Wang G, Das J, Eckert J. Acta Mater 2009;57:4133.
[9] Hufnagel TC, Ott RT, Almer J. Phys Rev B 2006:73.
[10] Egami T, Dmowski W, Kosmetatos P, Boord M, Tomida T, Oikawa E, et al. J Non-Cryst Solids 1995;193:591.
[11] Tomida T, Egami T. J Appl Phys 1991;69:5451.
[12] Tomida T, Egami T. Phys Rev B 1993;48:3048.
[13] Park KW, Lee CM, Wakeda M, Shibutani Y, Falk ML, Lee JC. Acta Mater 2008;56:5440.
[14] Lee SC, Lee CM, Lee JC, Kim HJ, Shibutani Y, Fleury E, et al. Appl Phys Lett 2008;92:151906.
[15] Lekka CE, Ibenskas A, Yavari AR, Evangelakis GA. Appl Phys Lett 2007;91:214103.
[16] Guan PF, Chen MW, Egami T. Phys Rev Lett 2010;104:205701.
[17] Plimpton S. J Comp Phys 1995;117:1.
[18] Kim YM, Lee BJ. J Mater Res 2008;23:1095.
[19] Arman B, Luo SN, Germann TC, Cagin T. Phys Rev B 2010;81:144201.
[20] Honeycutt JD, Andersen HC. J Phys Chem 1987;91:4950.
[21] Tsuzuki H, Branicio PS, Rino JP. Comp Phys Commun 2007;177:518.
[22] Mattern N, Schops A, Kuhn U, Acker J, Khvostikova O, Eckert J. J Non-Cryst Solids 2008;354:1054.
[23] Rountree CL, Vandembroucq D, Talamali M, Bouchaud E, Roux S. Phys Rev Lett 2009;102:195501.
[24] Caprion D, Matsui J, Schober HR. Phys Rev Lett 2000;85:4293.
[25] Zhang H, Srolovitz DJ, Douglas JF, Warren JA. Phys Rev B 2006;74:115404.
[26] Zhang H, Srolovitz DJ, Douglas JF, Warren JA. Acta Mater 2007;55:4527.
[27] Zhang H, Srolovitz DJ, Douglas JF, Warren JA. Proc Natl Acad Sci 2009;106:7735.
[28] Wang G, Mattern N, Pauly S, Bednarcik J, Eckert J. Appl Phys Lett 2009;95:251906.
[29] Cheng YQ, Cao AJ, Sheng HW, Ma E. Acta Mater 2008;56:5263.
[30] Launey ME, Kruzic JJ, Li C, Busch R. Appl Phys Lett 2007;91:051913.
[31] Haruyama O, Inoue A. Appl Phys Lett 2006;88:131906.
[32] Malandro DL, Lacks DJ. J Chem Phys 1999;110:4593.
[33] Cheng YQ, Sheng HW, Ma E. Phys Rev B 2008;78:014207.